Journal of Rock Mechanics and Geotechnical Engineering 14 (2022) 1642–1651

Contents lists available at ScienceDirect

Journal of Rock Mechanics and Geotechnical Engineering

journal homepage: www.jrmge.cn

Technical Note

An effective method for laboratory acoustic emission detection and location using template matching

Xinglin Lei [a,*], Tomohiro Ohuchi [b], Manami Kitamura [a], Xiaying Li [c,d], Qi Li [c,d]

[a] National Institute of Advanced Industrial Science and Technology (AIST), Tsukuba, 305-8567, Japan
[b] Geodynamics Research Center, Ehime University, Matsuyama, 790-8577, Japan
[c] State Key Laboratory of Geomechanics and Geotechnical Engineering, Institute of Rock and Soil Mechanics, Chinese Academy of Sciences, Wuhan, 430071, China
[d] University of Chinese Academy of Sciences, Beijing, 100049, China

A R T I C L E I N F O

Article history:
Received 31 August 2021
Received in revised form
7 February 2022
Accepted 15 March 2022
Available online 27 April 2022

Keywords:
Acoustic emission
Template matching and location
Waveform cross-correlation
Grid search

A B S T R A C T

In this paper, a template matching and location method, which has been rapidly adopted in microseismic research in recent years, is applied to laboratory acoustic emission (AE) monitoring. First, we used traditional methods to detect P-wave first motions and locate AE hypocenters in three dimensions. In addition, we selected events located with sufficient accuracy (normally corresponding AE events of relatively larger energy, showing clear P-wave first motion and a higher signal-to-noise ratio in most channels) as template events. Then, the template events were used to scan and match other poorly located events in triggered event records or weak events in continuous records. Through cross-correlation of the multi-channel waveforms between the template and the event to be detected, the weak signal was detected and located using a grid-searching algorithm (with the grid centered at the template hypocenter). In order to examine the performance of the approach, we calibrated the proposed method using experimental data of different rocks and different types of experiments. The results show that the proposed method can significantly improve the detection capability and location accuracy, and can be applied to various laboratory and in situ experiments, which use multi-channel AE monitoring with waveforms recorded in either triggering or continuous mode.

1. Introduction

Applications and researches involving acoustic emission (AE) monitoring have been performed for nearly a hundred years, and this method still has broad prospects in many fields. In the study of laboratory seismology, AE activity, as an analogue of seismicity, has been studied extensively. Many laws related to seismic activity have been verified and deepened from laboratory AE studies (see review in Lei and Ma, 2014). In the fields of geotechnical engineering and materials, AE technology has been continuously applied and developed (see review in Lei, 2017). With the needs of researches and applications, AE technology has shown progress in multiple directions in recent years. The rock samples used in the experiments for different purposes expand in two directions. On one hand, very small samples of a few millimeters in size were used in ultra-high-temperature and ultra-high-pressure compression tests and shed some light on the mechanism of deep earthquakes (Schubnel et al., 2013; Ohuchi et al., 2017). On the other hand, in the studies of faulting nucleation and hydraulic fracturing simulation, sub-meter- to meter-scale samples have been widely used (e.g. Ishida et al., 2013; Diaz et al., 2020; Yamashita et al., 2021). In terms of AE waveform recording, high-sampling-rate (up to 200 MHz), high-dynamic-range (16 bits), multi-channel AE systems have been developed and widely used in laboratory studies. AE waveforms can be recorded either in triggering mode or continuous mode. At the same time, these developments have brought about new challenges. In order to solve problems in practical engineering and academic researches encountered in recent years, an increasing number of experiments have been carried out using porous rocks, water-bearing rocks, and heat-treated rocks. Rock samples have been loaded under a fast loading rate, hydraulic fracturing, and indentation. In these cases, many AE signals are weak or noisy, and thus traditional data processing methods cannot achieve precise hypocenter location, which is the key dataset in many studies.

* Corresponding author.
E-mail addresses: xinglin-lei@aist.go.jp, xiaotianlei@gmail.com (X. Lei).
Peer review under responsibility of Institute of Rock and Soil Mechanics, Chinese Academy of Sciences.

https://doi.org/10.1016/j.jrmge.2022.03.010

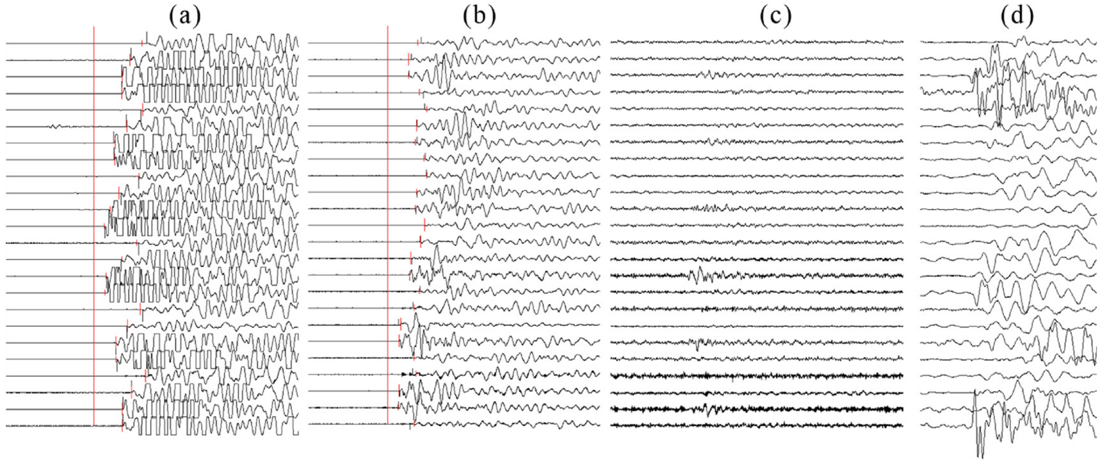

Fig. 1. Examples of 24-sensor AE waveforms with different S/N ratios: (a) Saturated waveforms of strong AE event; (b) Waveforms having clear P-wave first arrivals at all sensors; (c) Waveforms radiated from a weak event; and (d) Waveforms of an AE event that occurred in the tail of a previous event. Both events in (a) and (b) can be well located by the traditional method and are thus used as templates. Events in (c) and (d) cannot be precisely located by traditional methods. The long red lines in (a) and (b) indicate AE origin time, while short red and black lines indicate theoretical and detected P-wave arrival times, respectively.

In traditional AE data processing approaches, AE hypocenters have been determined routinely using the first arrival time data for P-wave and measured P-wave velocities during the test. First arrivals with a lower signal-to-noise ratio (S/N) are ruled out. If an AE event has weak P waves or a lower S/N, then its hypocenter cannot be determined. In particular, in water-saturated porous rocks, such as sandstone, numerous AE events cannot be precisely located due to weak first motions resulting from fast attenuation of high-frequency AE signals. In addition, during AE bursts, later events are normally disturbed by the tail of previous events. In these cases, traditional methods generally fail to detect and locate a large portion of AE events.

In recent years, matched filtering (or template scanning) technique based on cross-correlation of waveforms has been important in improving the detection capability of microseismic events and the accuracy of hypocenter determination. This method uses some well-located template events to detect small events by superimposing the cross-correlation function of waveforms for the template event and continuous records from multiple stations and components (Gibbons and Ringdal, 2006; Shelly et al., 2007a; Peng and Zhao, 2009). This method is improved later and then named the match and locate (M&L) method. In the M&L method, the stacking is performed after corrections of relative travel time which is calculated from the relative locations of the template event and potential event being searched through a three-dimensional (3D) mesh centered at the template (Zhang and Wen, 2015). The use of cross-correlation techniques to detect weak signals with similar waveforms is particularly effective for detection of similar signals with a low S/N ratio. Compared with traditional methods, this can extend the minimum magnitude of completeness of an earthquake catalog down by 1–2 units of magnitude (Meng et al., 2018; Ross et al., 2019; Wang et al., 2020). This is of great significance to seismological research, especially for various aspects of induced earthquake research, such as foreshock detection, early aftershock detection, fault-plane shape determination, and detection of low-frequency seismic events (Shelly et al., 2007b; Peng and Zhao, 2009; Skoumal et al., 2014).

The present study investigated the use of the M&L method to aid in the detection and hypocenter location of weak AE events on a laboratory scale. We herein described a modified M&L method for AE data and then presented examples by which to demonstrate the performance of the M&L method. Finally, we discussed issues related to matching parameters and template events selection.

2. Method

2.1. Multi-channel acoustic emission waveform monitoring

Fig. 1 shows four typical examples of multi-channel AE waveforms recorded during a rock fracture test. Cases (a) and (b) have a high S/N ratio and clear P-wave first motion and thus can be well located using traditional methods. For cases (c) and (d), the P-wave arrival times at most channels cannot be determined, and thus traditional AE data processing approaches fail in hypocenter determination. However, the M&L method is expected to be successful in detection and location of such events. In these examples, cases (a) and (b) can be used as template events.

2.2. Template-matching and location for multi-channel AE data

At first, the traditional approaches are applied for determination of the AE hypocenter. Then, only these well-located events are selected as templates. Finally, the M&L method is applied to detect and locate other events in either the event record or a continuous record. The flow of the M&L method is basically similar to that used for seismicity (Zhang and Wen, 2015), with some modifications to match the geometry of the rock sample and the characteristics of the AE signal. The general data processing procedure is as follows:

(1) P-wave arrival time pickup. The autoregressive (AR) model and Akaike information criterion (AIC) (Akaike, 1998) are used to determine the P-wave arrival time and its S/N ratio in each channel (Lei, 2017).
(2) Hypocenter determination. Determine AE hypocenters using the first arrival times of the P-wave at multiple sensors and measured P-wave velocities during the test. For most rocks, anisotropic velocities measured at different stages of deformation are required for better location precision. The first arrivals with an S/N ratio lower than a defined threshold are ruled out.
(3) Selection of template events. All precisely located events can be selected as templates. For later processes, it is necessary to add pickup and location data to template waveform files.

(4) Cross-correlation (CC) calculation. A running window of a given length is used to calculate the cross-correlation function for each template and event/continuous records in each channel.
(5) Potential hypocenters. For each template, the potential hypocenters are meshed in 3D (*X*-, *Y*-, and *Z*-direction) and centered at the template hypocenter, and the grid-search approach (following steps (6) and (7)) is designed to find the best hypocenter, which results in the maximum mean CC value.
(6) Time differences. The differences in P-wave arrival times for all grid cells are calculated for each channel between the template hypocenter and the potential hypocenters.
(7) Mean CC value and potential events. For each potential hypocenter, the cross-correlation is stacked with the time shift according to the time differences obtained in step (6). An event is detected when the stacked CC value and its S/N ratio exceed the predefined thresholds. After completing the grid search, the potential event with the largest CC value is retained and its magnitude is estimated based on the median value of the peak amplitude ratio between all channels of the detected event and the template.
(8) Detected events. Perform steps (6) to (8) for all templates. A potential event could be replaced, along with its location, by another location having a higher mean CC value. After scanning all of the templates, the potential event with the largest CC value will be the final detected event.

The detailed process for determining the P-wave arrival times can be found in Lei (2017). For convenience, we presented a summary herein. In this method, both the AE signal and background noise are represented using an AR model as a time series x_i ($i = 1, \ldots, N$):

$$x_i = \sum_{j=1}^{M} a_j x_{i-j} + u_i \ (i = 1, \ldots, N) \tag{1}$$

where M and a_j are the order and coefficients of the AR model, respectively; and u_i is the residual error. Parameters are estimated based on the AIC (Akaike, 1998) given by

$$AIC = -2\ln(l_{\max}) + 2M \tag{2}$$

where $l_{\max}$ is the maximum likelihood.

The point determining the P-wave arrival is the boundary between the background noise and the AE signal, and several algorithms to find this point have been proposed (e.g. Yokota et al., 1981). For AE signals, two algorithms, called MUPEO and MEPET, have been found to be practically useful (Satoh et al., 1987). In MUPEO, the F-model (of order M_F), which is obtained by applying the AR model to a small section (N points) at the head of the noise, is applied to the two sections separated at time k in the whole record. The AIC at running point k is given by

$$AIC_k = k\ln\left(\widehat{\sigma}_F^{\,2}\right) + (N-k)\ln\left(\widehat{\sigma}_{FS}^{\,2}\right) + N\ln(2\pi) + N + 2(M_F + 2) \tag{3}$$

where $\widehat{\sigma}_F^{\,2}$ and $\widehat{\sigma}_{FS}^{\,2}$ are the variances of the prediction error for the first and second sections, respectively.

In MUPET, the F-model is only applied to the first section, whereas the S-model (of order M_S), which is obtained for a small section (also N points) at the tail of the signal, is applied to the second section. The AIC at a running point k is then given by

$$AIC_k = k\ln\left(\widehat{\sigma}_F^{\,2}\right) + (N-k)\ln\left(\widehat{\sigma}_S^{\,2}\right) + N\ln(2\pi) + N + 2(M_F + M_S + 2) \tag{4}$$

where $\widehat{\sigma}_S^{\,2}$ is the variance of the prediction error for the second section.

We normally applied both MUPEO and MUPET, and chose the earlier pickup as the final arrival time, which better matched manual picking. The minimum AIC corresponds to the boundary between the noise and the signal, because the F-model only contains noise and the S-model only contains the signal. Based on our experience, a multi-step approach is especially effective. The MUPEO is first applied to the entire record for a preliminary estimation of the arrival time. Next, both MUPEO and MUPET are applied to a shorter time window centered at the estimated arrival time, and the earlier arrival time is used as the final estimation.

With arrival times at more than four channels, the hypocenter can be determined by linear inversion or global grid search methods. As a practical approach, we normally used a refining process. Once a primary hypocenter is determined, selection of the P-wave arrival time for channels can be reprocessed within a focused window centered at the theoretical arrival times. Then, the hypocenter is refined with the new arrival times. This procedure can be repeated several times until the best resolution is obtained.

In step (5), the normalized cross-correlation CC (k, t) (t: time) for the AE waveforms of two events at the k-th channel is given by (Meng et al., 2012)

$$CC(k,t) = \frac{\int_{-T}^{T}[W_1(k,\tau) - \overline{W_1}][W_2(k,t+\tau) - \overline{W_2}]\mathrm{d}\tau}{\sqrt{\int_{-T}^{T}[W_1(k,\tau) - \overline{W_1}]^2 d\tau}\sqrt{\int_{-T}^{T}[W_2(k,t+\tau) - \overline{W_2}]^2 \mathrm{d}\tau}} \tag{5}$$

Here, W_1 and W_2 represent the template waveform and the record to be detected, respectively; $\overline{W_1}$ and $\overline{W_2}$ are the means of W_1 and W_2 in the sliding window of length T, respectively. Generally, it is better to remove the mean from each sliding window to reduce the probability of false detection (Meng et al., 2012; Chamberlain et al., 2021). However, it has been reported that the normalized cross-correlation can reasonably be used without subtracting the mean for faster calculation (Beaucé et al., 2018). In our program, whether or not the mean is removed is an option. In step (7), the P-wave arrival time difference ($\Delta t(k)$) between the potential event and the template due to their location difference is directly calculated for all channels using the measured anisotropic P-wave velocities using a straight ray-path approximation. The mean CC value ($\langle CC(t) \rangle$) is then calculated by stacking CC (k, t) over K channels:

$$\langle CC(t) \rangle = \frac{\sum_{k=1}^{K} CC[k, t + \Delta t(k)]}{K} \tag{6}$$

In the M&L procedure, the control parameters should be defined according to the experimental configurations and characteristics of the observed AE signals, including (1) the size of the test sample, (2) the number and distribution of sensors, (3) the frequency range of AE signals, and (4) the duration time of typical AE events. The main control parameters include (1) the maximum time shift of the CC, (2) the time window for calculating the CC, (3) the frequency band of the filter, (4) the CC and S/N ratio threshold values for detecting an event, and (5) the search distance and number of grid cells along the *X*-, *Y*-, and *Z*-direction for the potential hypocenter. In general, the search distance for the potential hypocenter is approximately a few percent to approximately 20% of the sample size. A grid cell number of 10–20 along each direction is sufficient (see Sections 4.1 and 4.2).

Calculation of the correlation coefficient is the most time-consuming process in the M&L method. We adopted the algorithm and C code to achieve fast calculation of Eq. (5) by avoiding some repeated multiple operations, such as $W_2(k, t+\tau)W_2(k, t+\tau)$ (See Appendix A in Supplementary data).

In addition, we also compiled the M&L into an independent executable module, so that different parts of the waveforms (triggered event records or continuous records) to be scanned can be processed in parallel on a multi-core personal computer (PC) or on different PCs.

Figs. 2 and 3 show examples of detected AEs. The detected events are embedded in the tail of a previous event and cannot be located by traditional methods. However, the events can be detected and located by a template event using the M&L method. In Fig. 2, the high CC value of 0.88 indicates that the detected AE event and the template have very similar waveforms in most channels. Although the CC value in Fig. 3 is 0.52, the detected event along with its location is also acceptable, indicating that the defined CC threshold of 0.5 is reliable.

3. Results of validity verification

3.1. Application to high-P and high-T experiments using a deformation-DIA apparatus

Several groups have conducted deformation experiments using a deformation-DIA apparatus at ultra-high pressure (up to more than 1 GPa) and ultra-high temperature (up to more than 1000 K) conditions (Schubnel et al., 2013; Ohuchi et al., 2017) with AE monitoring in a similar setup, as shown in Fig. 4. AE signals were collected at six P-wave type piezoceramic transducers (PZTs) that were attached to the rear side of each second-stage anvil. The transducer was approximately 1 mm in thickness and approximately 4 mm in diameter, with a resonance frequency of approximately 2–4 MHz. Each transducer was electrically isolated from the second-stage anvils by a mirror-polished alumina disk (thickness of 0.5 mm). AE signals from the transducers were pre-amplified with a gain of 40 dB with a flat frequency response over the range of 100 Hz to 20 MHz and were then digitized and recorded using a high-speed multi-channel waveform recording system. This system can record AE waveforms at a sampling rate up to 100 MHz (16 bit, 8192 samples) in three working modes: single event, multi-event, and continuous mode. In the present study, we mainly used the

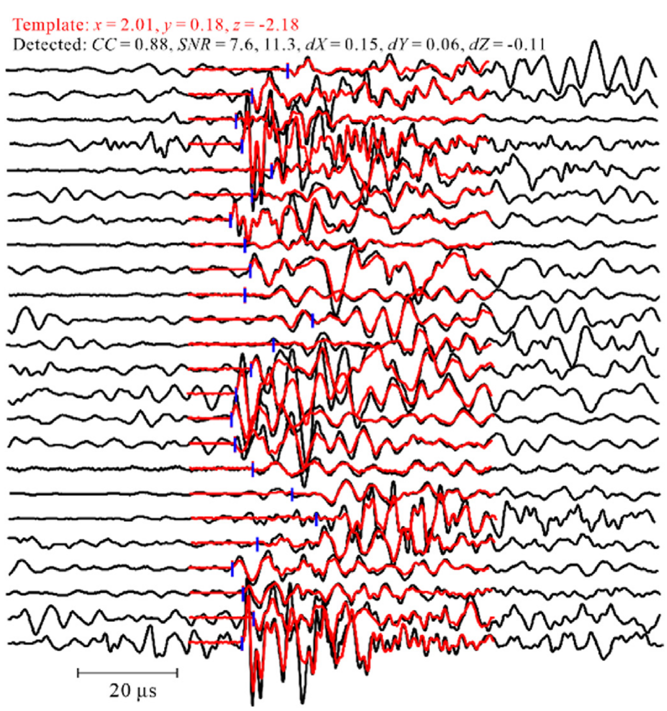

Fig. 2. Example of waveform matching and location. The waveforms of a smaller event (black) are overlapped by the tail of a previous event and thus cannot be located by traditional methods. The small event is precisely detected and located by a template event (red) using the M&L method. The stacked CC is 0.88, SNR means the mean signal to noise ratio, and *dX*, *dY*, and *dZ* show the location of the detected event relative to the template. The overlapped blue vertical bars indicate the matched P-wave arrival times.

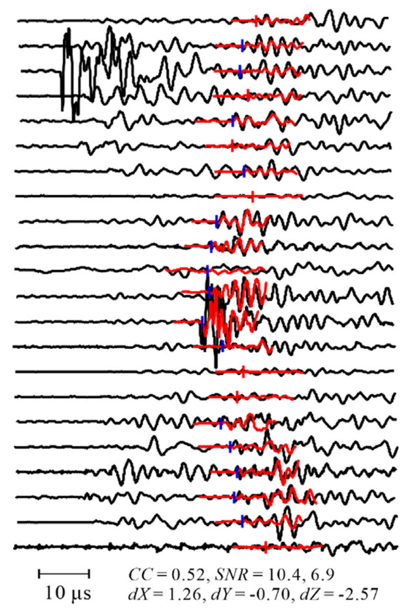

Fig. 3. Example of waveform matching. The overlapped blue/red vertical bars indicate the matched P-wave arrival times, in which traces of a blue bar were used in the hypocenter determination of the template event. See the caption of Fig. 2 for other details.

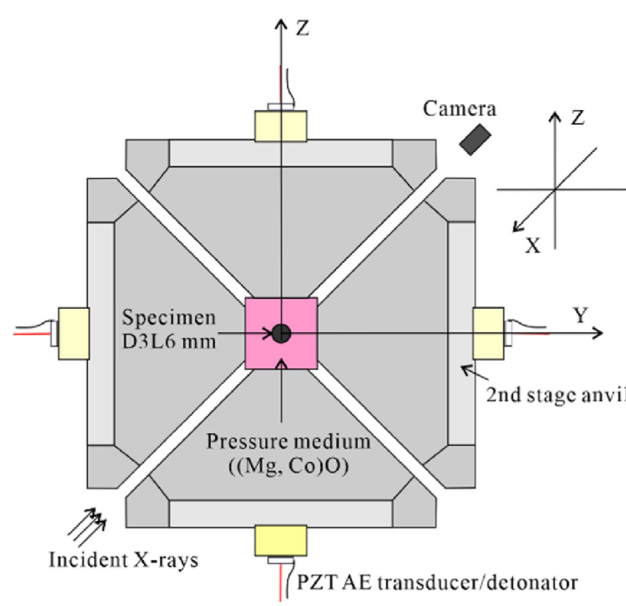

Fig. 4. Schematic diagram of transducer setup in deformation-DIA apparatus (modified from Ohuchi et al., 2017). The sample was shaped in cylinder of a diameter of 3 mm and a length of 6 mm (D3L6).

multi-event mode, in which the system can record up to approximately 5000 events per second and the digitized waveform data are directly stored in the onboard memory. The AE sensors function not only as receivers of AE signals but also as acoustic sources for measuring the velocity of an elastic wave during the test. Changes between being a receiver and detonator are controlled by a number of automatic switches.

In the experimental system, the six AE probes are symmetrically arranged along three orthogonal compression axes, and the distance from the probe to the sample is 60 mm, which is much larger than the sample size (diameter of 3 mm). Therefore, the bending of the ray path can be ignored, and the position of an AE hypocenter along the *X*-, *Y*-, and *Z*-direction can be determined separately based on the difference in the P-wave arrival times between each pair of sensors along each axial direction:

$$x_i = V_{\mathrm{P}i}\left(t_i^+ - t_i^-\right) \quad (i = X, Y, Z) \tag{7}$$

where $V_{\mathrm{P}i}$ is the measured P-wave velocity for the experimental sample along the *i*-th axis. Here, t_i^+ and t_i^- are the P-wave arrival times at sensors mounted in the positive and negative directions, respectively. The P-wave arrival time difference can be accurately determined by waveform cross-correlation. During the location process, the S/N ratios for the P-wave first motions are a measure of the location accuracy. An event can be located only when all six sensors have a clear first motion of an S/N ratio greater than 2.

Fig. 5 shows an example of located AE hypocenters in an olivine sample deformed at 900 °C (Ohuchi et al., 2018). In this experiment, the triggering mode was applied to recorded AE waveforms. During the experiment, the recording system will record waveform data when any triggering channel detects an AE signal (the signal threshold is slightly greater than the background noise level). In this way, a large number of events cannot be located. For example, 1000 events were recorded with waveforms. First, we tried to locate all events by the above method, but only 213 events were automatically located with reliable arrival times (S/N > 2) at all six

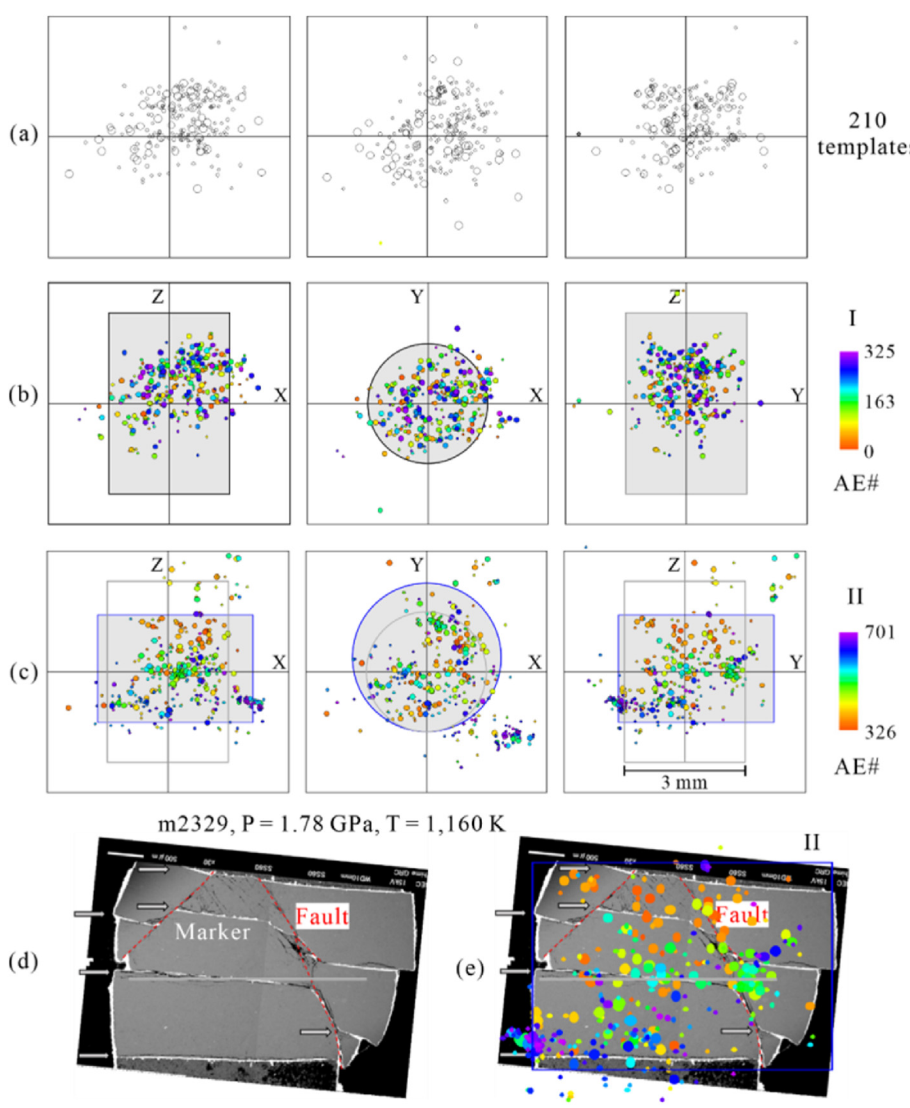

Fig. 5. Detected AE events during a triaxial compression test (referred as m2329) under a pressure of 1.78 GPa and a temperature of 1160 K using a deformation-DIA apparatus. In total, 490 events were detected and precisely located by 210 template events (a) using of the template-matching and location technique. (b) Distribution of 326 earlier events; (c) Distribution of the later 376 events; (d) SEM image of the deformed sample with major fractures indicated; and (e) Acoustic emission hypocenters overlapped on the SEM image. *P*: Pressure; *T*: Temperature.

Table 1
The main controlling parameters.

Parameters	Values
Maximum time shift of CC	0.3 μs
Time before P-wave	1 μs
Time after P-wave	3 μs
Inter-event time	25 μs
Frequency band of filter	[0.1 MHz, 3.0 MHz]
CC threshold value	0.5
S/N ratio threshold value	3
Search distance along *X*-, *Y*-, and *Z*-direction	0.5 mm/0.5 mm/0.5 mm

sensors. A total of 210 events satisfied the requirements of template events: the S/N ratio for the first P-wave motion is greater than 3 in all channels. Then, we used the waveforms of these template events to scan the waveforms of the remaining nearly 800 events and performed relative location via a grid search. The search range was 0.5 mm with a grid interval of 0.1 mm along the *X*-, *Y*-, and *Z*-direction. The thresholds of CC value and the S/N ratio were 0.5 and 3, respectively. The main controlling parameters are summarized in Table 1.

In the end, we obtained 702 reliable hypocenters (including the 210 template events), indicating that the M&L method is very powerful, and 490 events have been additionally located relative to their template event. The location of these hypocenters has a good correspondence with the fracture network revealed using a scanning electron microscope (SEM) after the test (Fig. 5). The observed AE activity indicates that the fluid-free dunnite undergoes brittle fracture under ultra-high temperature and ultra-high pressure conditions and gives a plausible mechanism for intermediate-depth earthquakes (Ohuchi et al., 2018).

3.2. *Application to rock fracture experiments under triaxial compression and fluid injection*

As a test, we applied the M&L method using AE data obtained in the laboratory of the Geological Survey of Japan. To date, the experimental and AE monitoring system in this laboratory is still representative. The following is a summary of the typical experiment setup and AE monitoring method. In order to record ultrasonic AE signals radiating from micro-cracking and stick-slip events, and as a pulse source for performing velocity measurements, up to 24 PZTs (diameter of 5 mm and resonance frequency of 2 MHz) were mounted on the curvilinear surface of the specimen using an epoxy agent. The specimens and two end pieces were coated with silicone sealant in order to prevent the confining oil from leaking into the specimens. The specimens can handle a total shear displacement of approximately 2 mm, which is sufficient for up to approximately 20 stick-slip events. The waveform recorder has 24 A/D channels with a sampling rate of up to 100 MHz, a dynamic range of 16 bits, and 256 mega words of onboard memory for each channel. The AE signal from each sensor is normally preamplified by 40 dB, digitized at a sampling rate of 10–100 MHz, and then recorded in either triggering mode or continuous mode. In the triggering mode, the system was triggered at a predefined threshold, and a logical operation was performed on signals from four to eight selected channels. The often-used triggering threshold is 25–50 mV, and the triggering logic is "#1 OR #2 OR #3 OR #4" and "(#1 OR #2) AND (#3 OR #4)". Here, #1, #2, #3, and #4 indicate the channels selected for triggering. Logic "#1 OR #2 OR #3 OR #4" means that waveform recording will be triggered when any selected channel meets a signal exceeding the threshold. In the continuous mode, the system can collect waveforms having a time span of approximately 20 s with a sampling rate of 10 MHz.

First, we tested the M&L method using the dataset obtained during a tri-axial compression test with water injection of tight sandstone. The preliminary motivation for this test is to examine the fracturing behavior of tight sandstone around the wet-dry boundary. First, the sample was hydrostatically compressed by increasing the confining pressure to 0.7 MPa. Distilled water was then injected from the bottom end at a constant injection pressure of 0.5 MPa. Water injection lasted for 18 h, and the waterfront reached the middle point of the sample, which was verified by real-time velocity measurements along multiple paths. The confining pressure and injection pressure were then increased to 22.5 MPa and 11.5 MPa, respectively. Finally, axial loading was applied at a constant rate of 5 MPa/min to 75 MPa, and at 1 MPa/min until specimen failed (peak stress: 137 MPa). The drained condition was maintained at a constant fluid pressure of 11.5 MPa at the bottom injection end, whereas the top end was kept at atmosphere pressure and the confining pressure was kept constant at 22.5 MPa during the entire axial loading process (Fig. 6).

Waveforms of the AE events from 24 sensors were recorded under triggering mode with the lowest triggering threshold and triggering logic of "#1 OR #2 OR #3 OR #4". In total, we observed more than 30,000 AE events. Many events could not be well located as they had no clear P-wave first motions at a sufficient number of sensors. As a result, among the 8336 events automatically located by traditional method, 1194 events were precisely located using at least 16 reliable P-wave arrival times (Fig. 7a and b). Many more events were poorly located with fewer arrival time data. Then, these well-located events were selected as template events to scan the remaining waveforms. The following gives the controlling parameters tested in Table 2, which can be considered as a standard example for similar experiments. (See Section 4.1 for matching parameter determination and the criteria used for template events selection).

As shown in Fig. 7, approximately 18,000 events were located or relocated with improved precision. There were 9714 additional events, which could not be located by the traditional method. It is valuable to note that the location error of AEs occurring on the surface of the sample is relatively large (1–2 mm at the center and 2–3 mm to the surface). As a result, there are some "air quakes" in return, i.e. an intuitive understanding of the location accuracy. In this dataset, we allowed the hypocenter to be located only 1 mm out of the rock sample.

Then, we used the M&L method to test the dataset of another experiment, in which water was injected from both ends of the sample, and the change from fluid-driven micro-cracking to fast fracturing-driven fluid flowing was observed (Li et al., 2016). In the experiment, we used a relatively higher triggering level, thus the total number of events with waveform data is lower than that in the previous example presented above. A total of 4739 events were located with P-wave arrival times at more than 11 sensors (Fig. 8a). After manual checking and re-selection, we obtained 5122 hypocenters determined by more than 11 arrival times (Fig. 8a). Among these events, 663 events satisfied the criteria for template event selection (more than 15 arrival times were used for location). Finally, more than 5000 events were re-located or newly located with the M&L method. As shown in Fig. 8, the relocated hypocenters outline more clearly the pattern of fractures. The earlier fluid diffusing process and the later fast fracturing process have also been revealed more clearly (Fig. 9). In addition to the ruptured shear fractures, which are visible from the computed tomography (CT) image just after the test, the AE hypocenter distribution revealed that in the middle of the rock sample, i.e. at the boundary between dry and wet regions (Li et al., 2016), an extensional jog was formed initially and finally became a macroscopic shear rupture and an extensional fault bend. Such experimental results are

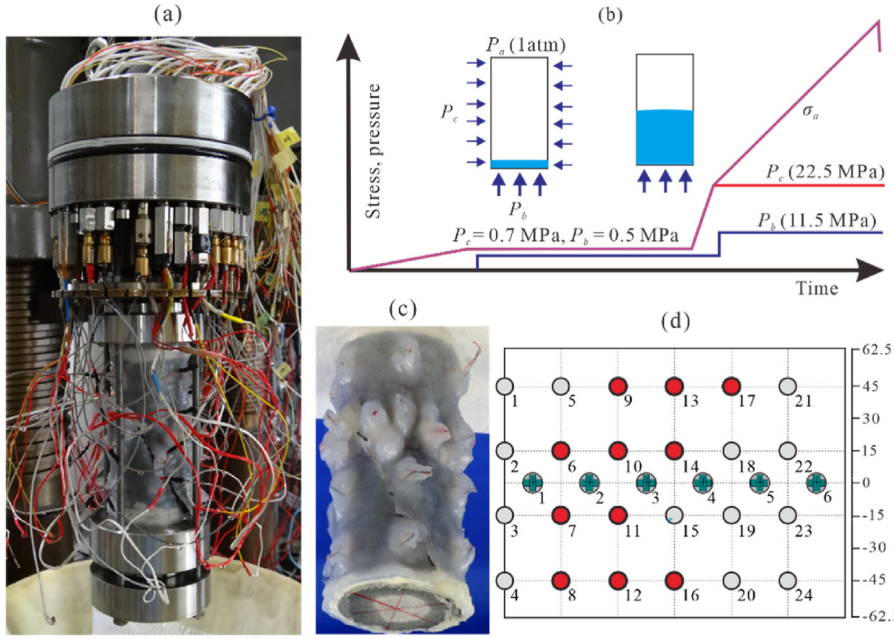

Fig. 6. (a) Photograph of the test specimen and connected signal lines after the experiment, (b) Schematic diagram for the injection and triaxial compression experiment, (c) Photograph of the failed specimen covered by silicone sealant, and (d) Distribution of 24 piezoelectric ceramic transducers (filled with red and grey colors) and six cross-type strain gauges (circles with a "+" symbol) affixed to the surface of the specimen. Sensors filled with red color and numbered 6 to 17 were also used as sources (connected to a pulse generator through program-controlled fast switches) for real-time velocity measurement along multiple paths. P_a, P_b: water pressure; P_c: confining pressure; σ_a: axial stress.

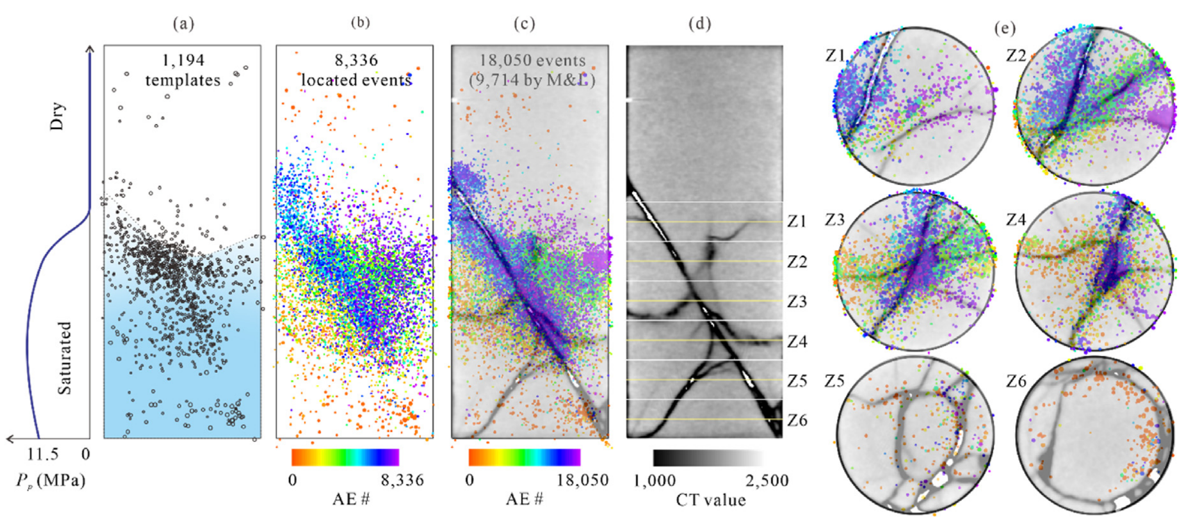

Fig. 7. Hypocenters of AE events induced by water injection in tight sandstone (see text for details). (a) Distribution of 1194 templates events, (b) AE hypocenters determined by the traditional method (the minimum number of P-wave arrival times is eight), (c) Distribution of all located events, including 9714 events detected and located by the M&L method, (d) X-Ray CT image of the fractured sample, cut along the vertical section perpendicular to major fractures. Hypocenters in (a), (b), and (c) are also projected on the same section, and (e) A collection of horizontal sections of CT images overlapped with AE hypocenters. The symbols of AE hypocenters were colored with sequential AE numbers. The side plot in Fig. 7a shows water pressure (P_p) profile.

helpful for understanding the formation of a fracture network induced by hydraulic fracturing.

4. Discussion

4.1. Template event selection and location error

The template events are selected based on the number of reliable travel times (M) that has been used in the hypocenter location. In principle, four travel times are sufficient to determine the hypocenter and the origin time of an AE event. However, errors in selecting data and the velocity model result in location errors. The value of M is a simple measure of hypocenter accuracy. In other words, the larger the value of M, the higher the accuracy. The travel times used for hypocenter determination must meet the following two conditions: (1) the S/N ratio must be greater than the specified threshold (e.g. 2 in our system), and (2) the difference from the theoretical travel time must be less than the specified value (i.e. 0.5 μs). For a specific dataset, we need to balance the number and hypocenter accuracy of the template events. In practical

Table 2
The controlling parameters tested.

Parameters	Values
Maximum time shift of CC	1–2 μs
Time before P-wave	2 μs
Time after P-wave	10 μs
Inter-event time	50–250 μs
Frequency band of filter	[0.1 MHz, 3 MHz]
CC threshold	0.5 (Fig. 7), 0.4 (Fig. 8)
S/N ratio threshold	2
Search distance	2.5 mm (Fig. 7), 6 mm (Fig. 8)

applications, one can first select template events with a larger *M*, and then add the detected events with good quality as additional templates for rescanning.

We did not deliberately remove the event of saturated waveforms from the templates. Since the template matching approach is based on waveform similarity, retaining such events will not cause adverse effects, and similar events can sometimes be matched. There are indeed some events having saturated waveforms that cannot be automatically located due to background noise, but can be matched by the M&L method.

We have performed P-wave velocity measurements along multiple paths many times during the experiment. The coordinates of the detonators are known, and thus the associated waveform data can be used to evaluate the location accuracy. In the experiment shown in Figs. 8 and 9, we used 12 sensors as detonators for velocity measurement, and carried out 1104 shots in total. As seen from the distributions of location error along the *X*-, *Y*-, and *Z*-direction, the M&L method significantly improves the location accuracy (Fig. 10). In the matching process, the first 12 shots were used as template events. We can see a trend of increasing error (see Fig. 11), which is resulted from changes in the P-velocity related to fluid diffusion and micro-cracking activity (Li et al., 2016).

In some experiments, a hole was drilled for water injection. Because the diameter of the hole is only 2 mm, which is much smaller than the dominant wavelength of the AE signal and wave

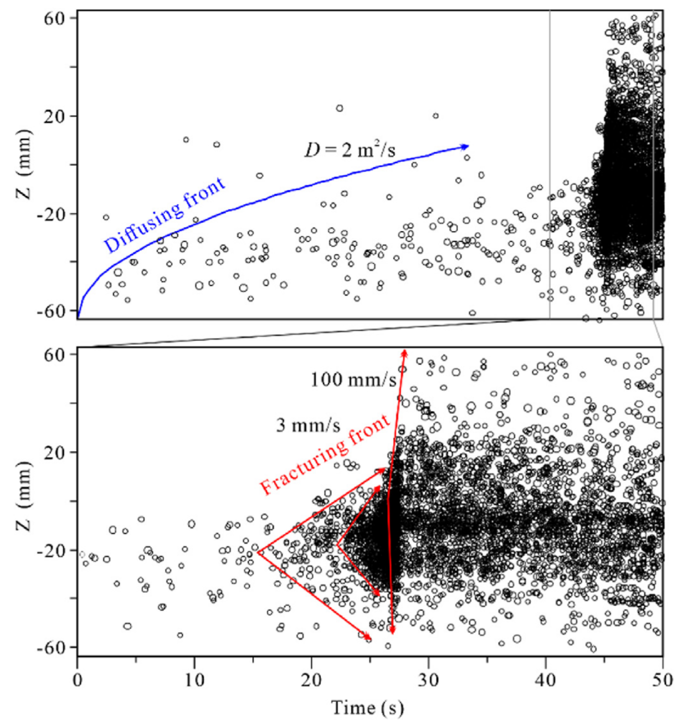

Fig. 9. Migration of AE hypocenters clearly revealing the transition process from fluid diffusion to rapid fracturing. *D*: Hydraulic diffusivity.

used for velocity measurement (for example, when the P-wave velocity is 5 km/s, the wavelength of 100–500 KHz wave is 10–50 mm), the influence of the water injection hole can be ignored.

4.2. Matching parameters

The test results of different datasets show that the CC threshold should be determined independently based on the characteristics

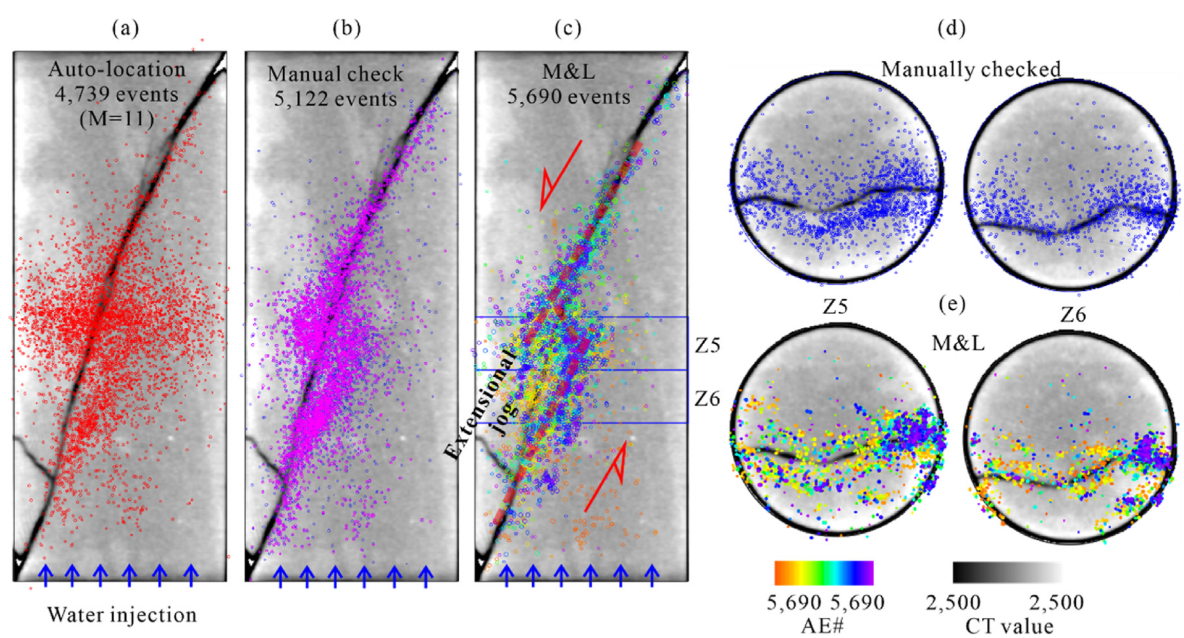

Fig. 8. Hypocenters of AE events induced by water injection in a tight sandstone (see text for details). (a) Distribution of 4739 automatically determined hypocenters by the traditional method, (b) AE hypocenters after manual checking and selection, (c) Total of 5690 hypocenters determined by the M&L method using 663 template events, and (d) and (e) Two horizontal sections of AE hypocenters. Hypocenters were overlapped on X-Ray CT image of the fractured sample. Hypocenters in (c) and (e) were colored with event number.

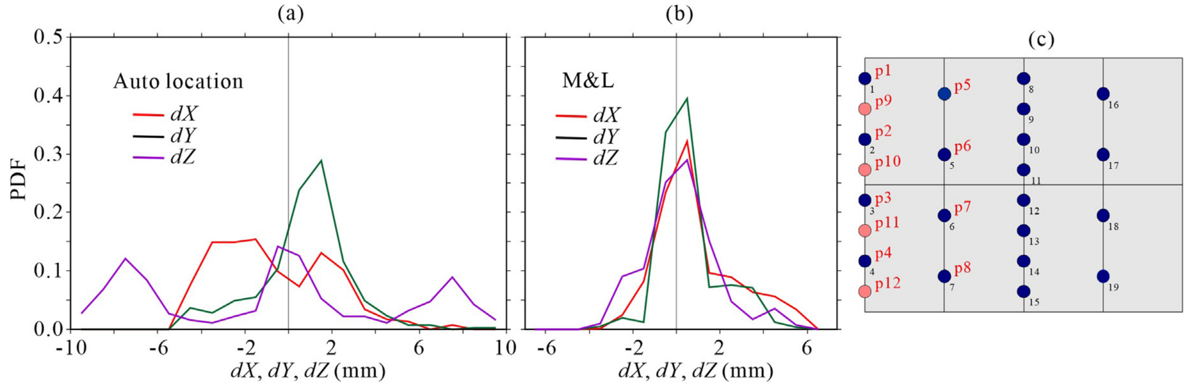

Fig. 10. Probability density function (PDF) of location error along X-, Y-, and Z-direction of shoot events. (a) Results of automatically determined hypocenters, (b) Results of templates and events located by the M&L method, and (c) Distribution of transducers affixed to the surface of the specimen. Blue circles indicate sensors used for AE monitoring. Sensors marked as p1, p2, ...p12 were used as detonators for velocity measurement, in which red colored ones were for velocity measurement only.

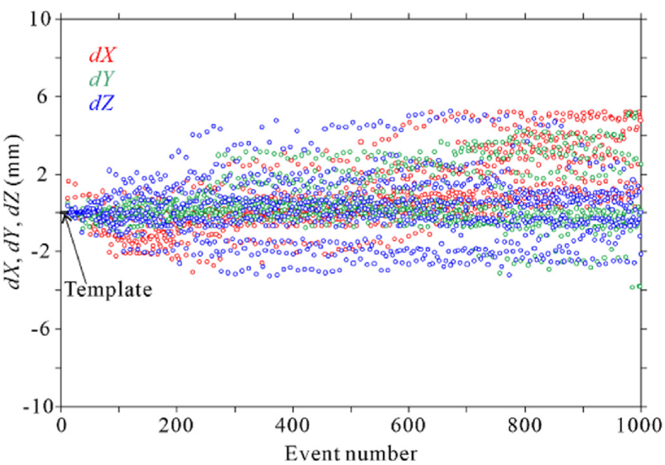

Fig. 11. Location errors (equal to shifts here) along X-, Y-, and Z-direction of shooting events relative to their template events. The first 12 shoots located at different positions of the sample surface, and their corresponding detonator coordinates were selected for template events. Increasing errors with increasing event numbers indicated the heterogeneous change of velocity from water diffusion and cracking activity.

of a given data set. In our cases, a CC threshold value of 0.4 is sufficient to avoid false detection. However, when the CC threshold value is less than 0.5, some events are located at the boundary of the given search distance range (we suggest a typical value of less than 1/5 of the sample dimension), and thus their hypocenter location is poorer (Fig. 12). For the S/N ratio of the template events, a value of 2.5–3 is a proper choice. In addition, calculating the S/N ratio and CC value of the newly detected events is also helpful to remove the false detections (Zhai et al., 2021).

It is noted that for the case of continuous records, the median absolute deviation (MAD) of the mean correlation coefficient trace for each template event (using N (e.g. $N = 8–12$) times the MAD as the detection threshold) is generally more robust than the absolute CC value (Shelly et al., 2007a; Peng and Zhao, 2009; Ross et al., 2019).

In addition to the above general principles, specific template selection criteria and scanning parameters must be determined through test runs of a given dataset obtained by different experimental configurations and recording systems.

5. Conclusions

We modified and applied the M&L method to experimental data of different rocks (including crystalline rock, sedimentary rock, and artificial rock) with different types of experiments (including an ultra-high temperature and pressure test with a deformation-DIA apparatus, a triaxial compression test, and a hydraulic fracturing test). Compared with traditional methods, many more events recorded with waveforms under the triggering mode could be relocated with improved precision. The proposed method is especially powerful for sedimentary rocks and hydraulic fracturing experiments as most AE events have relatively weak signals and could not be detected and located by traditional methods. Similar to the case of micro-seismic monitoring in the field, the M&L method is

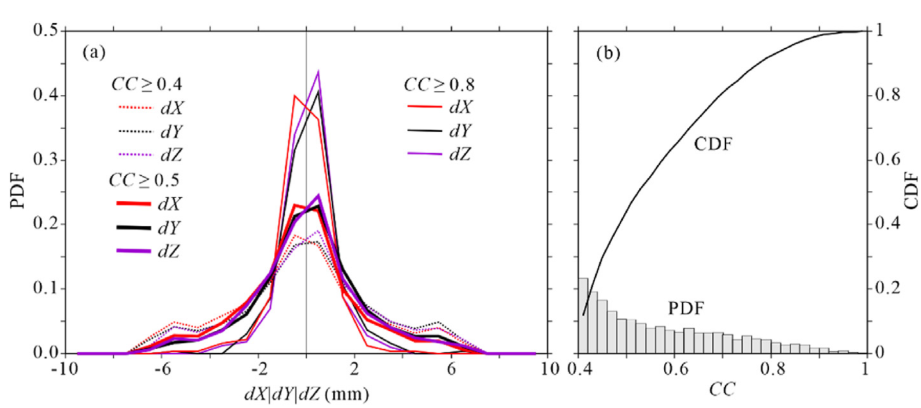

Fig. 12. (a) Probability density function (PDF) of distances in X-, Y-, and Z-direction of detected and located events related to templates, and (b) PDF of distances and cumulative density function (CDF) of detected event number as a function of CC.

more powerful for continuously recorded waveforms. Thus, continuously recording at multiple stations is also a preferable approach for AE hypocenter monitoring in the laboratory. However, for lower event rates, continuous recording is just a waste of disk space and time for data processing. Considering the practical usefulness, we proposed a multi-mode scheme for AE waveform recording, in which the triggering mode is normally applied for lower event rates, and continuous waveform recording is applied for higher event rates. The method and algorithm presented in the present article can be directly applied to other laboratory studies of different configurations and also to in situ experiments at meter scales.

Declaration of competing interest

The authors declare that they have no known competing financial interests or personal relationships that could have appeared to influence the work reported in this paper.

Acknowledgments

The authors thank the anonymous reviewers for their comments and suggestions. We acknowledge the funding support from Grant-in-Aid for Scientific Research (Grant No. 19H00722) by Japan Society for the Promotion of Science (JSPS).

Appendix A. Supplementary data

Supplementary data to this article can be found online at https://doi.org/10.1016/j.jrmge.2022.03.010.

References

Akaike, H., 1998. Information theory and an extension of the maximum likelihood principle. In: Parzen, E., Tanabe, K., Kitagawa, G. (Eds.), Selected Papers of Hirotugu Akaike. Springer Series in Statistics. Springer, New York, NY, USA.

Beaucé, E., Frank, W.B., Romanenko, A., 2018. Fast matched filter (FMF): an efficient seismic matched-filter search for both CPU and GPU architectures. Seismol Res. Lett. 89 (1), 165–172.

Chamberlain, C.J., Frank, W., Lanza, F., Townend, J., Warren-Smith, E., 2021. Illuminating the pre-, co-, and post-seismic phases of the 2016 m7.8 kaikōura earthquake with 10 years of seismicity. J. Geophys. Res. Solid Earth 126 (8), e2021JB022304.

Diaz, M.B., Kim, K.Y., Jung, S.G., 2020. Effect of frequency during cyclic hydraulic fracturing and the process of fracture development in laboratory experiments. Int. J. Rock Mech. Min. Sci. 134, 104474.

Gibbons, S.J., Ringdal, F., 2006. The detection of low magnitude seismic events using array-based waveform correlation. Geophys. J. Int. 165 (1), 149–166.

Ishida, T., Nagaya, Y., Inui, S., Aoyagi, K., Nara, Y., Chen, Y., Chen, Q., Nakayama, Y., 2013. AE monitoring of hydraulic fracturing experiments conducted using CO_2 and water. In: Proceedings of the ISRM International Symposium - EUROCK 2013. Wroclaw, Poland. ISRM-EUROCK, 2013-149.

Lei, X., Ma, S., 2014. Laboratory acoustic emission study for earthquake generation process. Earthq. Sci. 27 (6), 627–646.

Li, X., Lei, X., Li, Q., 2016. Injection-induced fracturing process in a tight sandstone under different saturation conditions. Environ. Earth Sci. 75, 1466.

Lei, X., 2017. Laboratory acoustic emission study review. In: Rock Mechanics and Engineering, vol. 2. CRC Press, Boca Raton, FL, USA, pp. 127–164.

Meng, X., Yu, X., Peng, Z., Hong, B., 2012. Detecting earthquakes around salton sea following the 2010 Mw7.2 el mayor-cucapah earthquake using GPU parallel computing. Procedia Comput. Sci. 9, 937–946.

Meng, X., Chen, H., Niu, F., Tang, Y., Yin, C., Wu, F., 2018. Microseismic monitoring of stimulating shale gas reservoir in SW China: 1. An improved matching and locating technique for downhole monitoring. J. Geophys. Res. Solid Earth 123 (2), 1643–1658.

Ohuchi, T., Lei, X., Ohfuji, H., Higo, Y., Tange, Y., Sakai, T., Fujino, K., Irifune, T., 2017. Intermediate-depth earthquakes linked to localized heating in dunite and harzburgite. Nat. Geosci. 10, 771–776.

Ohuchi, T., Lei, X., Higo, Y., Tange, Y., Sakai, T., Fujino, K., 2018. Semi-brittle behavior of wet olivine aggregates: the role of aqueous fluid in faulting at upper mantle pressures. Contrib. Mineral. Petrol. 173 (10), 88.

Peng, Z., Zhao, P., 2009. Migration of early aftershocks following the 2004 parkfield earthquake. Nat. Geosci. 2, 877–881.

Ross, Z.E., Trugman, D.T., Hauksson, E., Shearer, P.M., 2019. Searching for hidden earthquakes in Southern California. Science 364 (6442), 767–771.

Satoh, T., Kusunose, K., Nishizawa, O., 1987. A minicomputer system for measuring and processing AE waveform-high speed digital recording and automatic hypocenter determination. Bull. Geol. Surv. Jpn. 38 (6), 295–303 (in Japanese).

Schubnel, A., Brunet, F., Hilairet, N., Gasc, J., Wang, Y., Green, H.W., 2013. Deep-focus earthquake analogs recorded at high pressure and temperature in the laboratory. Science 341 (6152), 1377–1380.

Shelly, D.R., Beroza, G.C., Ide, S., 2007a. Non-volcanic tremor and low-frequency earthquake swarms. Nature 446 (7133), 305–307.

Shelly, D.R., Beroza, G.C., Ide, S., 2007b. Complex evolution of transient slip derived from precise tremor locations in western Shikoku. Japan. Geochem. Geophys. Geosys. 8 (10). https://doi.org/10.1029/2007gc001640.

Skoumal, R.J., Brudzinski, M.R., Currie, B.S., Levy, J., 2014. Optimizing multi-station earthquake template matching through re-examination of the Youngstown, Ohio, sequence. Earth Planet Sci. Lett. 405, 274–280.

Wang, Z., Lei, X., Ma, S., Wang, X., Wan, Y., 2020. Induced earthquakes before and after cessation of long-term injections in Rongchang gas field. Geophys. Res. Lett. 47 (22), e2020GL089569.

Yamashita, F., Fukuyama, E., Xu, S., Kawakata, H., Mizoguchi, K., Takizawa, S., 2021. Two end-member earthquake preparations illuminated by foreshock activity on a meter-scale laboratory fault. Nat. Commun. 12 (1), 1–11.

Yokota, T., Zhou, S., Mizoue, M., Nakamura, I., 1981. An automatic-measurement of arrival-time of seismic-waves and its application to an online processing system. Bull. Earthq. Res. Inst. Univ. Tokyo 56, 449–484.

Zhai, Q., Peng, Z., Chuang, L.Y., Wu, Y.M., Hsu, Y.J., Wdowinski, S., 2021. Investigating the impacts of a wet typhoon on microseismicity: a case study of the 2009 typhoon Morakot in Taiwan based on a template matching catalog. J. Geophys. Res. Solid Earth 126 (12), e2021JB023026.

Zhang, M., Wen, L., 2015. An effective method for small event detection: match and locate (M&L). Geophys. J. Int. 200, 1523–1537.

Dr. Xinglin Lei is a senior researcher of seismology and geomechanics at National Institute of Advanced Industrial Science and Technology (AIST) in Japan. He graduated from China University of Geosciences in 1983 and then obtained his MSc and PhD degrees from Institute of Geology, China Earthquake Administration (CEA). He has been involved in research on seismology and geomechanics for more than 25 years. In recent years, he has conducted integrated research using multiple methods (laboratory experiments, field surveys, and numerical simulations) on multi-scale (core- and field-scale) with focuses on fault reactivation and induced seismicity by fluid injection in areas such as geological disposal of CO_2, shale gas hydraulic fracturing, and enhanced geothermal systems.